LA-UR-18-22397
Approved for public release; distribution is unlimited.

Title: Fluid Mechanics of an Obliquely Mounted MIV Gauge

Author(s): Bdzil, John Bohdan

Intended for: This document is intended to be a replacement of LA-13380-MS which is listed as a LA-Report in the library but can not be located.
Report

Issued: 2018-03-21

Fluid Mechanics of the Obliquely Mounted MIV Gauge-(John B. Bdzil)

I. Introduction

"Over the 40-yr history of shock-compression science, numerous physical phenomena have been considered for use in detecting wave profiles. Few of the devices have actually been used for a significant and persistent study. Part of this history is connected to the difficulty in actually developing a credible device."[1] These remarks from Graham summarize the current state of in situ particle gauge technology. Uncertainties arising from the affect that gauge response time, perturbation to the flow, calibration, and reproducibility have on accurate in situ measurements are not completely understood. If the error in accuracy resulting from these uncertainties is of order of 5%, the physical phenomena can still be the basis of a useful technique. With increased understanding, sensible corrections for such errors could be made. As of this time, no technology has surfaced as the clear choice for such a gauge.

At Los Alamos, magnetic gauges are the technology of choice. The obliquely mounted Magnetic Impulse Velocity (MIV) gauge first introduced by Fowles[2] and popularized by Vorthman and Wackerle[3] has been used @ DF-site for over a decade to make in situ measurements of lagrangian particle velocity in inerts and explosives. Recently Gustavsen, Sheffield, and Alcon[4] have observed that these gauges do not provide an accurate measure of the particle velocity in liquids. The purpose of this report is to describe the response on shock loading of an obliquely mounted thin inert slab imbedded in a inert whose density and compressibility are different from that of the slab. Obliquity is measured relative to the shock normal direction in the imbedding inert.

This study assumes perfect fluid response (i.e., no viscous etc. effects). The conclusions that I draw from this study are:

(1) the pressure obtained in the initial shock loading is different in the slab and imbedding material,

(2) pressure equilibrium is obtained quickly between the inert slab and the imbedding material (the system reaches hydrostatic equilibrium), which in turn affects the density ratio (ρ/ρ_0) in the slab, from which it follows by the Bernoulli law that,

---

[1] "Solids Under High-Pressure Shock Compression," R. A. Graham, Springer-Verlag, Berlin, 1993, p.62-5.

[2] "Experimental Technique and Instrumentation," by G. R. Fowles appearing in Dynamic Response of Materialsto Intense Impulsive Loading, edited by P. C. Chou and A. K. Hopkins, Air Force Materials Laboratory (1972).

[3] "Reaction Rates from Electromagnetic Gauge Date," by J. Vorthman, G. Andrews and J. Wackerle appearing in Eighth Symposium on Detonation, Albuquerque, July 15-19, 1985, p. 99-110.

[4] "Response of Inclined Electromagnetic Particle Velocity Gauges in shocked Liquids," by R. Gustavsen S. Sheffield and R. Alcon appearing in (1993) APS Proceedings.

(3) the vector particle velocity in the slab and imbedding material are not equal.

Stated somewhat differently, the underlying compressible fluid hydrodynamics does not support the operation of an obliquely mounted "particle" gauge unless the equation of state (eos) properties of the gauge and imbedding material are either identical or enjoy a unique relation. The successful operation of these gauges depends on a non-hydrostatic environment and possible transverse stresses (viscosity related) across the slab-imbedded material interface. To date, no study of these effects has been completed. Further study is needed before the MIV gauge results can be reliably interpreted.

This report is divided into three sections. In Section II, I give a brief history of the MIV gauge and the basic problem geometry and hydrodynamic equations for the flow. The specific example of a gauge that is aligned with the flow is considered in Section III. In Section IV, I give results for the measured particle velocity as a function of initial gauge angle. The conclusions drawn from this study are presented in Section V.

II. History and Problem Geometry

Twenty-three years ago Fowles[5] proposed a modification of the Dremin stirrup electromagnetic velocity gauge that could be used to provide a direct measure of momentum (pressure) rather than particle velocity. A key ingredient in the operation of the gauge is that the plane of the gauge not be coincident with the plane of the shock (i.e., the problem is inherently multi-dimensional). Figure 1 from Fowles[2] article, shows a side-on view of his momentum gauge, and Figure 2 shows a top view of the deflected, shock-compressed gauge. The operation of the gauge is described in ref. [2] along with a caution; "the theory of the gauge operation assumes that the oblique cut in the sample, along which the sensing element is placed, not perturb the wave being studied and that no slippage occur between the specimen material and the gauge. Limitations due to these possible effects are not yet established." Building on the ideas of Fowles, Vorthman and Wackerle[3] constructed a multi-element gauge that could be used to simultaneously measure particle velocity (stirrup probe) and stress (Fowles probe) at a number of different lagrangian locations. One advantage of their technique is that one experiment yields the data that previously required many experiments using the established techniques; thus shot-to-shot variations were eliminated.

A key to the operation of such a gauge is that the gauge needs to be obliquely mounted. To my knowledge no theoretical analysis was done of this multi-dimensional flow problem. Rather a number of symmetrical impact experiments, using a plastic as the imbedding material, were performed to confirm the efficacy of the technique. Based

[5] "An Electromagnetic Stress Gage," by C. Young, R. Fowles and R. Swift appearing in Proceedings of Sagamore Conference on Shock Waves and Mechanical Properties of Solids, Army Mechanics and Materials Research Center, 1970.

largely on the positive results obtained in those few experiments,[6] the technique was adapted for routine use and is now widely used at DF-site.

In October, 1992 I learned that Gustavsen and Sheffield were seeing a discrepancy between the expected and observed particle velocity. When the MIV gauge package was used in liquids such as nitromethane, the measured particle velocity was both lower than expected and a function of the initial gauge angle, (see Figure 2). The calculations I report on now were done in November, 1992. My goal was to gain an understanding of the fluid mechanics of the obliquely mounted MIV gauge.

II .1 gauge geometry and coordinates

The problem geometry is shown in Figure 3. Teflon is used as the gauge substrate. The variables and coordinate transformations used are:

variables

D_o ≡ unperturbed shock velocity in fluid,
U_p ≡ unperturbed supporting piston velocity,
V_{ph} ≡ phase velocity of unperturbed shock along unperturbed Teflon interface ≡ $D_o/\sin\phi$
P ≡ pressure
ρ ≡ density
ρ_o ≡ initial density

where the + subscript denotes the shock state, and

coordinate transformations

undeflected gauge basis vectors $\hat{e}_1 = \hat{i}\sin\phi - \hat{j}\cos\phi,\ \hat{e}_2 = \hat{i}\cos\phi + \hat{j}\sin\phi$

deflected gauge basis vectors $\hat{e}_\eta = \hat{i}\sin(\phi-\theta) - \hat{j}\cos(\phi-\theta),\ \hat{e}_\xi = \hat{i}\cos(\phi-\theta) + \hat{j}\sin(\phi-\theta)$

so that

$$\hat{i} = \hat{e}_\xi \cos(\phi-\theta) + \hat{e}_\eta \sin(\phi-\theta)$$

$$\hat{j} = \hat{e}_\xi \sin(\phi-\theta) - \hat{e}_\eta \cos(\phi-\theta)$$

and where the piston velocity is

[6] Private communication (1986), J. J. Dick

$$\bar{U}_p = U_p\left\{\hat{e}_\xi \sin(\phi-\theta) - \hat{e}_\eta \cos(\phi-\theta)\right\}.$$

A simple kinematic argument can be used to get the velocity of the gauge, $\bar{U}_g$. Assuming that the flow normal to the gauge is just equal to the component of U_p from the inert flow, $-U_p\cos(\phi-\theta)$, then

$$\begin{aligned}\bar{U}_g &\equiv \hat{e}_\xi U_\xi - \hat{e}_\eta U_p \cos(\phi-\theta)\\ &= \hat{i}\left\{U_\xi \cos(\phi-\theta) - U_p \cos(\phi-\theta)\sin(\phi-\theta)\right\}\\ &+ \hat{j}\left\{U_\xi \sin(\phi-\theta) + U_p \cos^2(\phi-\theta)\right\}.\end{aligned}$$

The $\hat{j}$ component of $\bar{U}_g$ is the measured gauge velocity. Once U_ξ is determined the velocity measured by the gauge is determined. If $U_\xi = U_p \sin(\phi-\theta)$ (i.e., the component of U_p in the $\hat{e}_\xi$ - direction) then the gauge measures U_p, the desired result. What I show is that

$$U_\xi \neq U_p \sin(\phi-\theta).$$

I assume that the flow is governed by the two-dimensional Euler equations. Transforming these equations to a reference frame that moves with speed (in the $\hat{e}_\xi$ – direction)

$$V = D_0/\sin(\phi-\theta),$$

at an angle $(\phi-\theta)$ with respect to the plane of the undisturbed inert shock (i.e., in the direction of the deflected gauge), and assuming that the flow is steady in this reference frame, yields

$$\underline{\text{mass}} \qquad \bar{\nabla}\cdot(\rho\bar{U}) = 0,$$

$$\underline{\text{2-momentum}} \qquad \bar{U}\cdot\bar{\nabla}(\bar{U}) = -\frac{1}{\rho}\bar{\nabla}P,$$

$$\underline{\text{energy}} \qquad \bar{U}\cdot\bar{\nabla}(e) - \left(P/\rho^2\right)\bar{U}\cdot\bar{\nabla}P = 0,$$

where

$$\bar{\nabla} = \hat{e}_\eta\frac{\partial}{\partial\eta} + \hat{e}_\xi\frac{\partial}{\partial\xi},$$

$$\bar{U} = \hat{e}_\eta U_\eta + \hat{e}_\xi\left(U_\xi - D_0/\sin(\phi-\theta)\right),$$

and U_η, U_ξ are the velocity components in the η and ξ directions, P is the pressure, ρ is the density, and $e(P,\rho)$ is the specific internal energy. In the standard fashion, these equations can be rewritten to get the differential form of the Bernoulli law

$$\bar{U}\cdot\bar{\nabla}\left\{e+P/\rho+\tfrac{1}{2}U_\eta^2+\tfrac{1}{2}(U_\xi-D_0/\sin(\phi-\theta))^2\right\}=0,$$

and in isentropic regions the energy equation can be solved to get P vs ρ along an isentrope

$$P_S(\rho).$$

For purposes of this demonstration, I'll assume a simple polytropic eos in both the gauge and surrounding inert and use the same polytropic exponent, for both

$$e = P/\rho/(\gamma-1),$$

and

$$P/\rho^\gamma = f(S),$$

where S is the entropy. The initial density of the two materials is of course different and these variables along with the gauge angle, ϕ control the solutions that I find. The analysis I report here can easily be extended to a more general $e(P,\rho)$ eos. I give the results for a Mie-Gruneisen fluid at the end of the Section III.

III. The 90° Gauge

The simplest example of an oblique gauge is one that is parallel to the flow (at right angles to the plane of the shock). Figure 4 shows a snapshot of this gauge geometry. Assuming that the only significant entropy generation in the Teflon occurs at the lead shock, it follows that

$$P/\rho^\gamma = \frac{2\rho_{0T}D_0^2\cos^2\omega}{\gamma+1}\left(\frac{\gamma-1}{(\gamma+1)\rho_{0T}}\right)^\gamma,$$

where the subscript T refers to Teflon. The differential form of the Bernoulli law states

$$e+P/\rho+\tfrac{1}{2}U_\eta^2+\tfrac{1}{2}(U_\xi-D_0/\sin(\phi-\theta))^2 = \text{constant}$$

along streamlines. For this geometry the constant is the same constant on every streamline, so that I get

$$e+P/\rho+\tfrac{1}{2}U_\eta^2+\tfrac{1}{2}(U_\xi-D_0)^2=\tfrac{1}{2}D_0^2.$$

Using the P/ρ^γ rule on the isentrope and a polytropic eos, it follows that in the Teflon

$$\frac{4\gamma D_0^2 \cos^2\omega}{(\gamma+1)^2}\left(\frac{P}{P_+}\right)^{\frac{\gamma-1}{\gamma}} + U_\eta^2 + \left(U_\xi - D_0\right)^2 = D_0^2.$$

For this geometry, $U_\eta \approx 0$ either on the axis or far downstream from the initial interaction with the lead inert shock. Since the acoustic communication times correspond to just a few reverberations of the gauge, it follows that far downstream (a distance of a few gauge thickness') the pressure is equilibrated and equal to the pressure behind the shock in the inert

$$P = \frac{2\rho_{0I} D_0^2}{\gamma+1},$$

where ρ_{0I} is the initial (unshocked) density of the inert, and we use the same adiabatic exponent γ for both the Teflon and the inert. Using this value for P, it then follows that

$$U_\xi = D_0\left\{1 - \sqrt{1 - \frac{4\gamma\cos^2\omega}{(\gamma+1)^2}\left(\frac{\rho_{0I}}{\rho_{0T}\cos^2\omega}\right)^{\frac{\gamma-1}{\gamma}}}\right\}.$$

This is the particle velocity measured by the gauge.

In order to test this theoretical result and also to get more information about the near gauge flow in the inert, I did a two-dimensional numerical simulation of this problem using the Los Alamos, second-order accurate Godunov hydrocode, CAVEAT.[7] For this comparison I used the parameter values

Teflon: $\rho_{0T} = 2.15 g/cc,\ \gamma = 7$

inert: $\rho_{0I} = 1.12 g/cc,\ \gamma = 7$

$\begin{pmatrix} "nitromethane" \\ case\ 1 \end{pmatrix}$ $D_0 = 4\ mm/\mu s,\ U_p = 1\ mm/\mu s$

inert: $\rho_{0I} = 1.8 g/cc,\ \gamma = 7$

$\begin{pmatrix} "HMX" \\ case\ 2 \end{pmatrix}$ $D_0 = 4\ mm/\mu s,\ U_p = 1\ mm/\mu s.$

and

[7] "CAVEAT: A computer code for Fluid Dynamics with Large Distortions and Internal Slip," Los Alamos Report, LA-10613, (1990).

inert: $\rho_{0I} = 3.33 g/cc,\ \gamma = 7$

$\begin{pmatrix} CH_2I_2 \\ case\ 3 \end{pmatrix}$ $D_0 = 4\ mm/\mu s,\ U_p = 1\ mm/\mu s.$

Both the axial particle velocity and the pressure contours obtained from the CAVEAT simulations of these problems are shown in Figures 5 and 6 and 7 for cases 1 and 2 and 3, respectively. From these figures, it is clear that after a short, high velocity transient, the particle velocity plateaus at a value considerably below the piston speed $U_p = 1 mm/\mu s$, for cases 1 and 2 and above for case 3. Comparing the plateau values obtained in the simulations with the result of evaluating our theoretical expression

$$U_\xi = D_0 \left\{ 1 - \sqrt{1 - \frac{4\gamma}{(\gamma+1)^2} \left(\frac{\rho_{0I}}{\rho_{0T}} \right)^{\frac{\gamma-1}{\gamma}}} \right\},$$

I find good agreement

	Steady Theory	CAVEAT
Case 1	0.536 $mm/\mu s$	0.54 $mm/\mu s$
Case 2	0.839 $mm/\mu s$	0.84 $mm/\mu s$.
Case 3	1.588 $mm/\mu s$	1.48 $mm/\mu s$.

Therefore in the extreme case of $\phi = 90°$, the difference between the velocity of the slab and the true particle velocity, $U_p = 1\ mm/\mu s$ can be very large. In the limit $\rho_{0T} = \rho_{0I}$ (recall that we assumed identical γ's for the gauge and inert) the gauge and inert are identical materials, which yields $U_\xi = 1\ mm/\mu s$.

To understand the dominant role played by the density ratio, (ρ_{0I}/ρ_{0T}), consider the following result. The above expression can be generalized to account for different polytropic exponents in the Teflon, γ and the inert, $\tilde{\gamma}$

$$U_\xi = D_0 \left\{ 1 - \sqrt{1 - \frac{4\tilde{\gamma}}{(\tilde{\gamma}+1)^2} \frac{\gamma(\tilde{\gamma}+1)^2}{\tilde{\gamma}(\gamma+1)^2} \left(\frac{\rho_{0I(\gamma+1)}}{\rho_{0T(\tilde{\gamma}+1)}} \right)^{\frac{\gamma-1}{\gamma}}} \right\}.$$

Using this result we can determine the conditions under which the observed and actual particle velocities would be identical, $U_\xi = 2D_0/(\tilde{\gamma}+1)$. This occurs when

$$\frac{\rho_{0I}}{\rho_{0T}} = \frac{(\tilde{\gamma}+1)}{(\gamma+1)}\left(\frac{\tilde{\gamma}(\gamma+1)^2}{\gamma(\tilde{\gamma}+1)^2}\right)^{\frac{\gamma}{\gamma-1}}.$$

The deformation of the Teflon slab (thickness) can be calculated by using the results for U_ξ and ρ obtained above and integrating the mass conservation equation

$$\bar{\nabla}\cdot(\rho\bar{U}) = 0$$

over the shaded region in Figure 4. The example shown in Figure 4 depicts the case of a high density slab surrounded by lower density inert. Performing the integration, yields

$$\frac{\langle U_\xi \rho\rangle}{\langle\rho\rangle} = D_0\left(1 - \frac{\rho_{0T}}{\langle\rho\rangle}\frac{l_{in}}{l_{out}}\right),$$

where $\langle\ \rangle$ denotes an average taken in the η-*direction* over the horizontal boundary of the region. Thus the relative thickness of the shocked gauge is

$$\frac{l_{out}}{l_{in}} = \frac{D_0\rho_{0T}}{D_0\langle\rho\rangle - \langle U_\xi\rho\rangle},$$

which on assuming a weak η-*dependence* for ρ and U_ξ becomes

$$\frac{l_{out}}{l_{in}} = \frac{\rho_{0T}}{\rho_T}\left(\frac{1}{1-U_\xi/D_0}\right).$$

We can use the expression to determine how the thickness of the driven slab changes. For the simple example of polytropic materials with identical polytropic exponents, l_{out}/l_{in} is

$$\frac{l_{out}}{l_{in}} = \frac{\left(\frac{\gamma-1}{\gamma+1}\right)\left(\frac{\rho_{0I}}{\rho_{0T}}\right)^{\frac{1}{\gamma}}}{\sqrt{1-\frac{4\gamma}{(\gamma+1)^2}\left(\frac{\rho_{0I}}{\rho_{0T}}\right)^{\frac{\gamma-1}{\gamma}}}}.$$

Provided that the flow in the gauge is subsonic (look ahead for the definition of the sonic parameter) l_{out}/l_{in} is an increasing function of (ρ_{0I}/ρ_{0T}). When $\rho_{0I} = \rho_{0T}$ we have l_{out}/l_{in}, while for $\rho_{0I} > \rho_{0T}$ we have $l_{out} > l_{in}$. Thus the typical case for explosives, $\rho_{0I} < \rho_{0T}$ leads to a thinning of the embedded gauge. For the case 3, CH_2I_2 inert example, this expression predicts the observed thickening of the gauge.

We can rewrite the general expression for l_{out}/l_{in} to get the material property independent result

$$(U_\xi)_I - (U_\xi)_T = \left(\frac{\rho_0}{\rho}\right)_T \frac{l_{in}}{l_{out}} - \left(\frac{\rho_0}{\rho}\right)_I .$$

If the slab is to be an accurate gauge, then $(U_\xi)_I \cong (U_\xi)_T$. This expression shows that we have three "variables" at our disposal to help achieve the desired equality of velocities:

$$\left(\frac{\rho_0}{\rho}\right)_T \cdot \left(\frac{\rho_0}{\rho}\right)_I ,$$

and l_{out}/l_{in}. For the simple polytropic fluid system (identical γ's), the change in density of the slab occurs via two steps: (1) shock loading to

$$\rho_T = \rho_{0T}\left(\frac{\gamma+1}{\gamma-1}\right)$$

followed by (2) an isentropic transformation to a state of pressure equilibrium with the imbedding inert

$$\rho_T = \rho_{0T}\left(\frac{\gamma+1}{\gamma-1}\right)\left(\frac{\rho_{0I}}{\rho_{0T}}\right)^{1/\gamma} .$$

Thus the compression of slab and inert are different and

$$(U_\xi)_I - (U_\xi)_T = \left(\frac{\gamma-1}{\gamma+1}\right)\left\{\frac{l_{in}}{l_{out}}\left(\frac{\rho_{0T}}{\rho_{0I}}\right)^{\frac{1}{\gamma}} - 1\right\}.$$

For the typical Teflon-based gauge (slab) imbedded in explosive (inert), $\rho_{0I} < \rho_{0T}$. Thus to get $(U_\xi)_I \cong (U_\xi)_T$ would require $l_{in} < l_{out}$, which is not likely. Perhaps the anisotropic nature of thin polymeric slabs such as Teflon could be used to some advantage here to control (l_{out}/l_{in}) and $\left(\frac{\rho_0}{\rho}\right)_T$, independently. This remains to be seen. This is a very compelling, rather general argument. It does not depend on the assumed inviscid nature of the flow. Thus it would appear that the basic physics does not favor the operation of the oblique gauge.

I've repeated all of these calculations using a Mie-Gruneisen equation of state for a Teflon slab and various imbedding inerts. The material constants and results are shown below:

Hugoniot: $U_s = C_0 + S\,U_p$

	$\rho_0(g/cc)$	$C_0(mm/\mu s)$	S	$(\rho\Gamma)$
Teflon	2.15	1.68	1.79	1.69
nitromethane	1.123	1.3	1.62	----
PMMA	1.18	2.55	1.65	----
CH_2I_2	3.33	1.25	1.65	----

Table I. Equation of State data

	$(\rho/\rho_0)_I$	$(\rho/\rho_0)_T$	$(U_\xi)_T(mm/\mu s)$
nitromethane	1.52	1.26	0.525
PMMA	1.31	1.31	0.611
CH_2I_2	1.53	1.46	1.760

Table II. Calculated results for U_p = *1 mm/μs*

A Fortran code is available to do these calculations.

The large discrepancy between the desired and calculated velocity for case 1 and 2 when $\phi = 90°$ argues that we either need to substantially increase the specific energy of the shocked Teflon so as to get a higher compression or that we increase the "effective" ℓ_{out} so that $\ell_{out} > \ell_{in}$. A quick calculation using the Bernoulli flow model described above shows that the sonic parameter

$$\left(U_\xi - D_0\right)^2 - C^2 = D_0{}^2\left\{1 - \frac{2\gamma\cos^2\omega}{(\gamma+1)}\left(\frac{p}{p_+}\right)^{\frac{\gamma-1}{\gamma}}\right\} < 0\,,$$

is less than zero (i.e., the flow relative to the shock is subsonic). Therefore, the region where the lead shock sits in the Teflon can be influenced by the flow near the leading edge of the Teflon. At least two simple routes exist by which energy can be transferred into the Teflon slab; Option (1) normal forces applied on the narrow end of the slab, and Option (2) tangential forces (viscosity related) applied on the large faces of the slab.

The CAVEAT simulations show very little pressure gradient near the leading edge of the Teflon. Thus, we anticipate that the inert/Teflon interface is Rayleigh-Taylor stable (i.e., the interface area will not grow). This combined with the small area of this region, argue against this as an important region to consider. Thus, Option (1) does not offer a viable mechanism for "densifying" the Teflon.

The current simulations do not admit tangential forces across the large faces of the slab because we dealt only with Euler fluids. When tangential forces due to viscous forces are allowed, it seems highly unlikely that the pressures in the Teflon could be increased to the point that a large amount of additional compression could be achieved. The more likely possibility would be a Kelvin-Helmholtz type instability along the interface. The net affect of such an instability would be to "wrinkle" the Teflon slab, thereby making ℓ_{out} effectively larger than ℓ_{in}. This seems like the only plausible scenario for getting $(U_\xi)_T \approx (U_\xi)_I$.

However, something about a "wrinkled" gauge seems very unattractive!

IV. "Small" ϕ Oblique Gauge

The solution to the oblique gauge problem can be obtained with a simple extension of the $\phi = 90°$ problem considered in the previous section (see Figure 8). As before, we have a Bernoulli law

$$e + P/\rho + \tfrac{1}{2} U_\eta^2 + \tfrac{1}{2} (U_\xi - D_0 / \sin(\phi - \theta))^2 = \tfrac{1}{2} (D_0 / \sin(\phi - \theta))^2,$$

along a streamline. Again assuming that the principal entropy generation in the Teflon occurs at the lead shock (see Figure 8), it follows that

$$P/\rho^\gamma = constant$$

along streamlines (different constants for different streamlines). This isentropic treatment of the flow along gauge streamlines neglects the weak wave reflections that occur behind the lead shock. The lead shock in the Teflon is oblique with respect to the lead, driving shock in the inert. For the case of supersonic flow depicted in Figure 8, the state of the lead shock in the Teflon is obtained by doing an oblique shock match with an incident inert shock having an attack angle ϕ.

A new variable appears in the oblique gauge problem: the gauge turning angle, θ. The initial value of θ is given by the oblique shock matching calculation. Gustavsen, Sheffield, and Alcon[4] give the asymptotic value of θ as

$$\tan(\phi - \theta) = \left(\frac{\rho_0}{\rho}\right)_I \tan \phi .$$

I have done the oblique matching problem for a number of different ϕ for the model system

$D_0 = 4mm/\mu s$, $\gamma = 3$
$\rho_{0T} = 2.15g/cc$, $\rho_{0I} = 1.12g/cc$.

The results of these calculations are shown in Table III. For this range of angles

ϕ	θ_{inert} / θ_{asymp}	$(P_+)_T$
30°	12°/14°	12GPa
40°	15°/17°	12GPa
20°	8°/10°	12GPa
10°	4°/5°	11GPa

Table III. - Oblique shock matching results

of attack, ϕ the shock pressure in the Teflon is relatively independent of ϕ and equal to $(P_+)_T = 12\ GPa$ and $(\rho_+)_T = 4.3\ g/cc$. Using these values in the isentrope and Bernoulli expressions, yields

$$U_\xi = \frac{D_0}{\sin(\phi-\theta)}\left\{1-\sqrt{1-\left(\frac{\sin(\phi-\theta)^2}{D_0}\right)\frac{2\gamma}{\gamma-1}\left(\frac{P_+}{\rho_+}\right)_T\left(\frac{P}{P_+}\right)_T^{\frac{\gamma-1}{\gamma}}}\right\}.$$

Again assuming pressure equilibrium between the inert fluid and Teflon slab (the gauge)

$$\left(\frac{P}{P_+}\right)=\frac{8.96}{12}$$

gives the results shown in Table IV, where

$$U_{gauge} = U_\xi \sin(\phi-\theta) + U_p \cos^2(\phi-\theta).$$

ϕ	θ	$(\phi-\theta)$	$U_\xi(mm/\mu s)$	$U_{gauge}(mm/\mu s)$
0°	0°	—	—	2
10°	4°	6°	0.09	1.99
20°	8°	12°	0.18	1.95
30°	12°	18°	0.27	1.89
40°	15°	25°	0.37	1.80
<90°>	0°	90°	1.13	1.13

Table IV. The measured values of U_{gauge} *(true value; $U_{gauge} = 2mm/\mu s$)*

Therefore, for this simple Euler fluid model we find that for the typical 30° gauge angle, we have an error of -5% in the measured velocity. If U_ξ was set identically to zero

(corresponding to no gauge motion in the ξ-*direction)* the error would be -10%. Thus for the 30° gauge geometry the maximum error we could realize is about -10%.

V. Conclusions:

The mass conservation argument presented in Section III shows that the first order physics of the oblique gauge is not favorable for its reliable operation. For a $\phi = 30°$ gauge this can lead to an order 5% error in the velocity measurement. Second order physics (such as viscosity, strength, non-isotropic material response) could lead to improved agreement between the calculated and desired response of the gauge. However, the time scale for these phenomena is usually slow compared to the μs time scale of interest, which is why we often neglect this physics. If they turn out to be important, their time scale could easily be comparable to the time scale of interest in our measurements. Should the "wrinkled" gauge effect discussed in Section III be important, it would probably be irreproducible.

From the arguments given above, it appears that the second order physics of the gauge/imbedding material pair need to be properly tuned to have a successful oblique gauge. It is therefore difficult to imagine how such a gauge could give an accurate measurement of the flow in a reacting explosive. Properties, such as viscosity, etc. can change significantly in going from unreacted to reacted explosive.

Some suggestions:

(1) study reacting explosives at several gauge angles,

(2) adjust gauge spacing so that same particles are sampled at all gauge angles,

(3) $\phi = 90°$ is the best geometry to study the physics of the oblique gauge, and

(4) use calculations to help understand the $\phi = 90°$ experiments.

Until we have a better understanding of the oblique MIV gauge, user beware. Perhaps the standard, non-oblique stirrup probe would be the best near term alternative. This problem deserves some careful experimental and theoretical study.

FIGURES

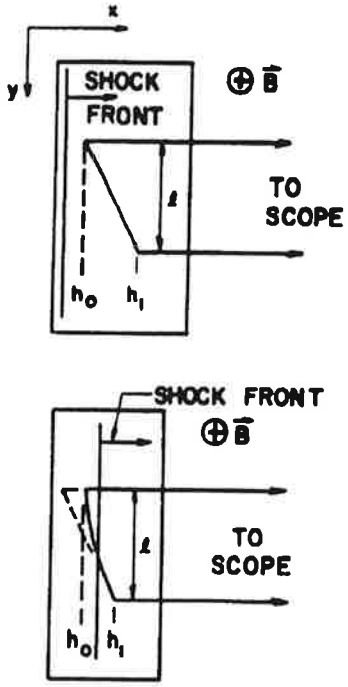

Figure 1. Electromagnetic stress gauge technique. (a) prior to shock arrival (b) during shock transit of sensing element (side-on view).

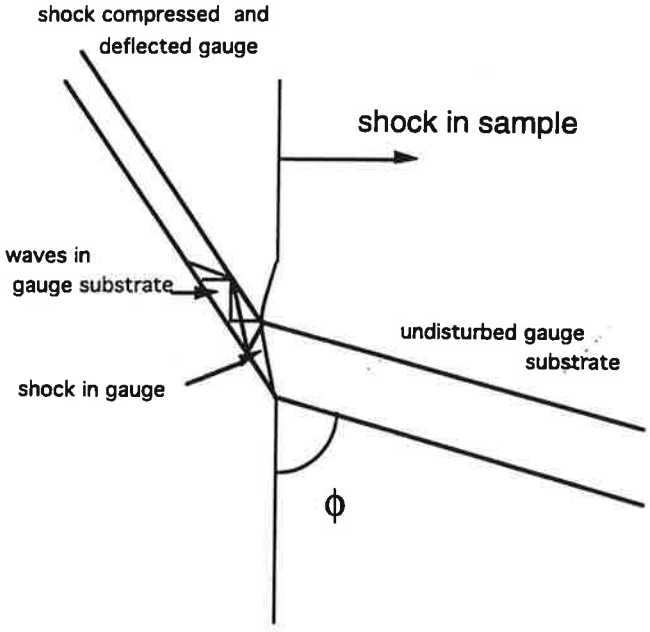

Figure 2. Electromagnetic stress gauge (top view). The plane of the gauge is deflected by the interaction.

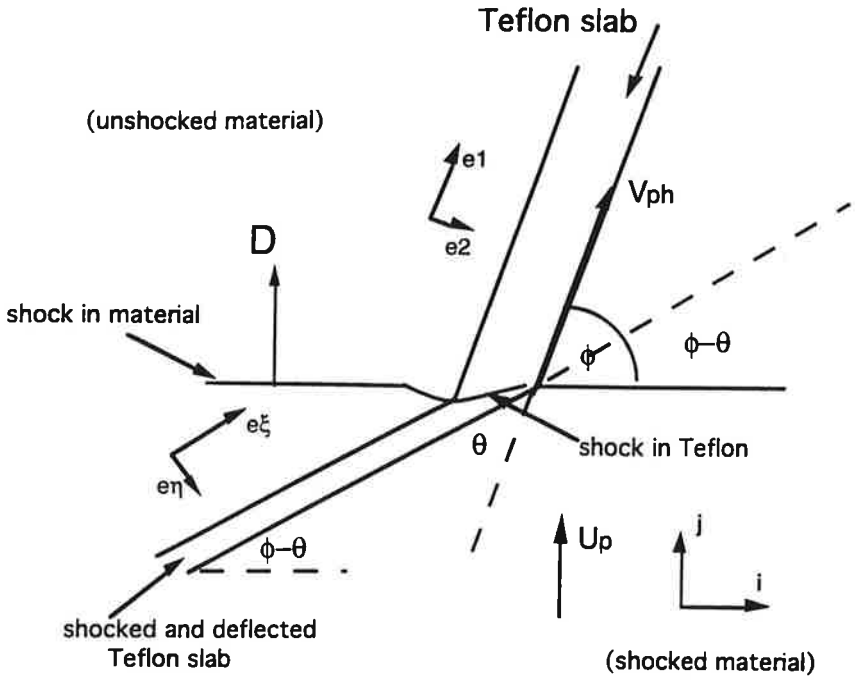

Figure 3. The geometry and coordinate frames for the MIV gauge analysis.

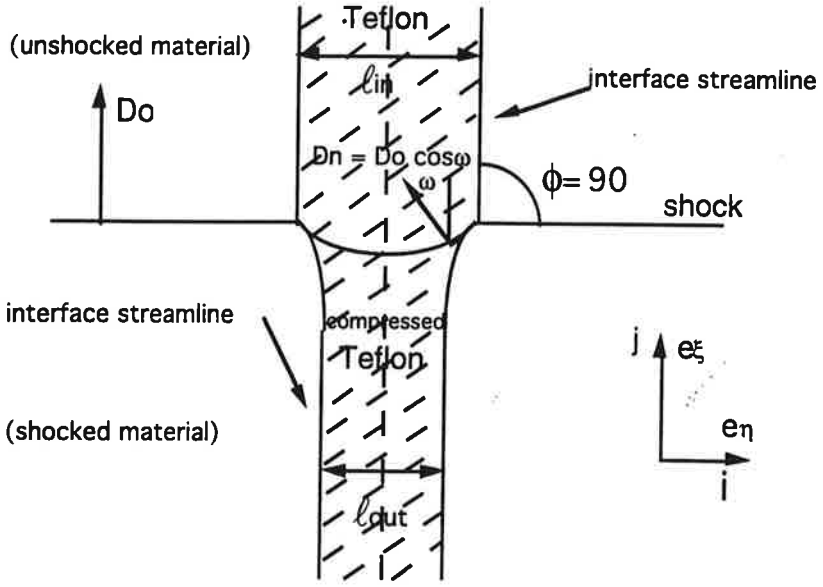

Figure 4. The simple, symmetric $\phi = 90°$ gauge problem. Shown is the case where ρ_o of the Teflon gauge is greater than ρ_o of the surrounding inert (the typical case).

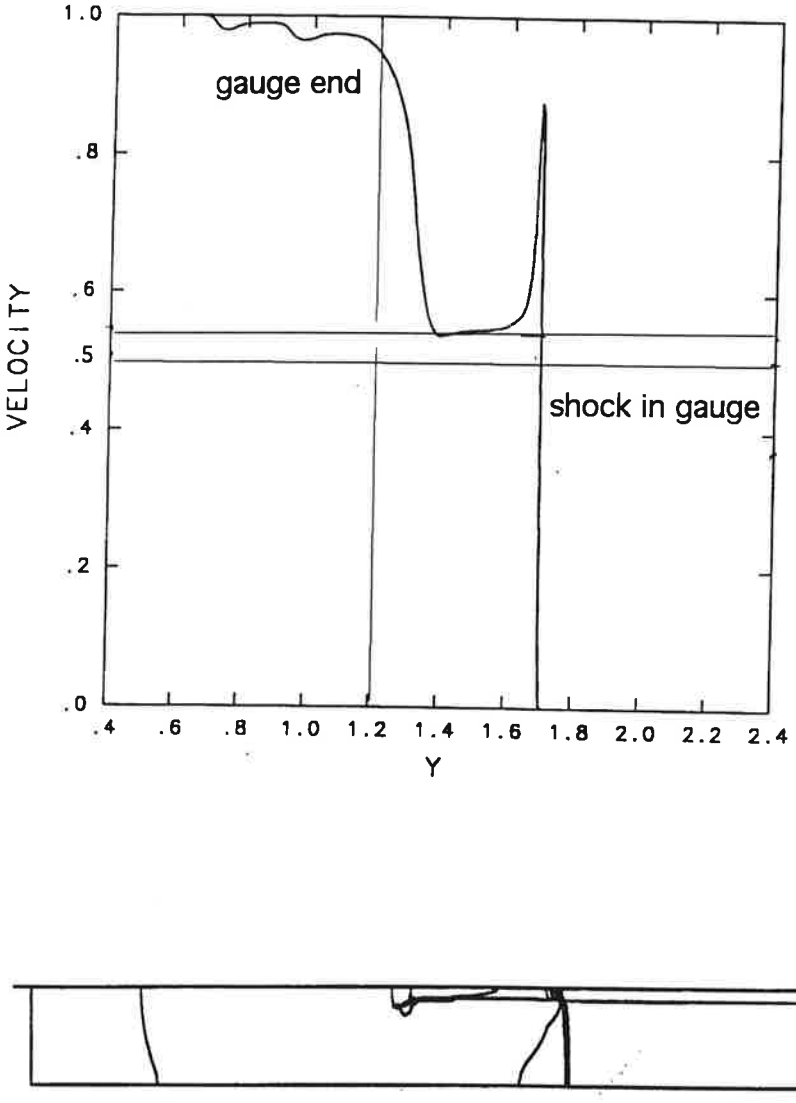

Figure 5. The particle velocity along the centerline of the $\phi = 90°$ gauge at $t = 0.43\mu s$ for case 1. is shown in Fig. 5a. The pressure contours for the $\phi = 90°$ gauge at $t = 0.43\mu s$ for case 1. is shown in Fig. 5b. The lack of pressure contours shows that pressure equilibirum is a good assumption.

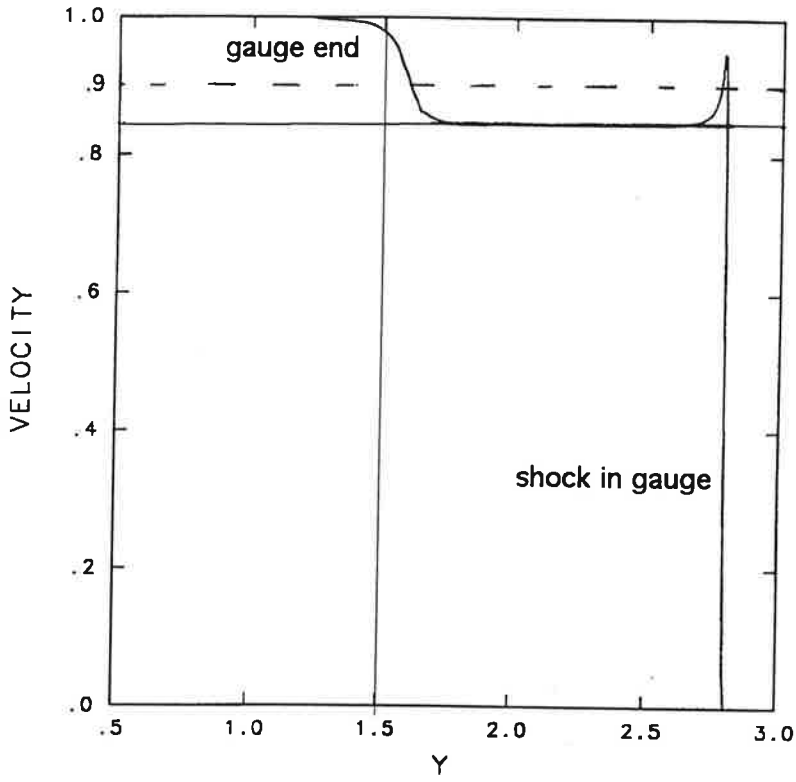

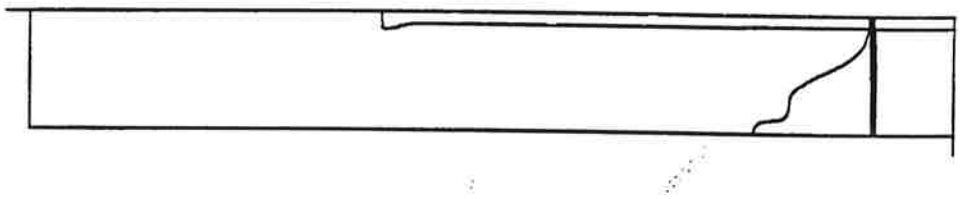

Figure 6. The particle velocity along the centerline of the $\phi = 90°$ gauge at $t = 0.7\mu s$ for case 2. is shown in Fig. 6a. The pressure contours for the $\phi = 90°$ gauge at $t = 0.7\mu s$ for case 2. is shown in Fig. 6b.

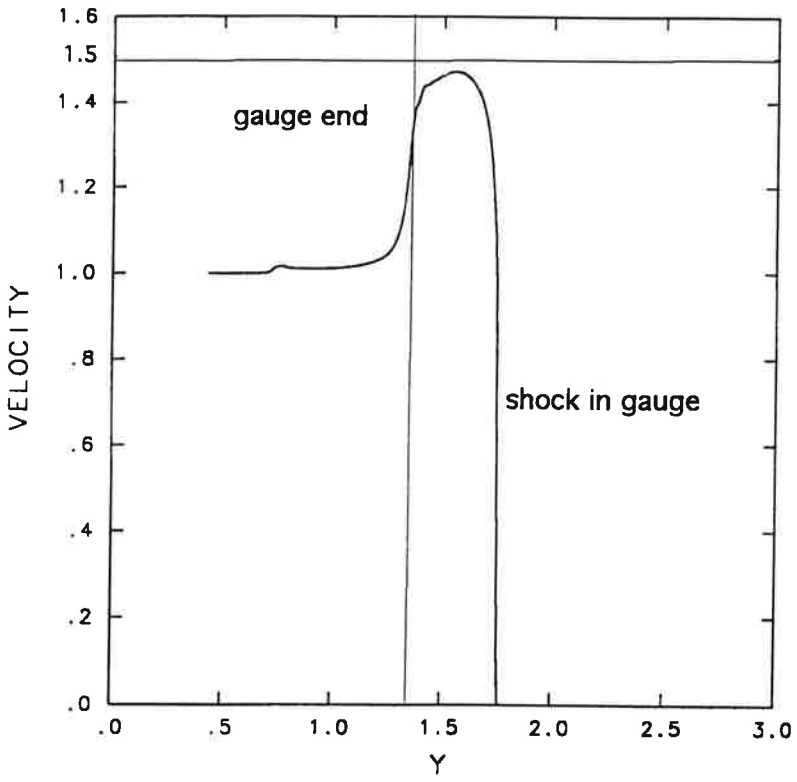

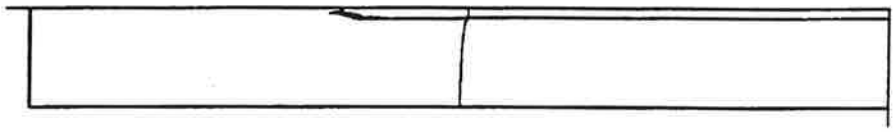

Figure 7. The particle velocity along the centerline of the $\phi = 90°$ gauge at $t = 0.43\mu s$ for case 3. is shown in Fig. 7a. The density contours for the $\phi = 90°$ gauge at $t = 0.43\mu s$ for case 3. is shown in Fig. 7b. Note that the shock leads in the gauge and that the shocked gauge is thicker than the unshocked gauge.

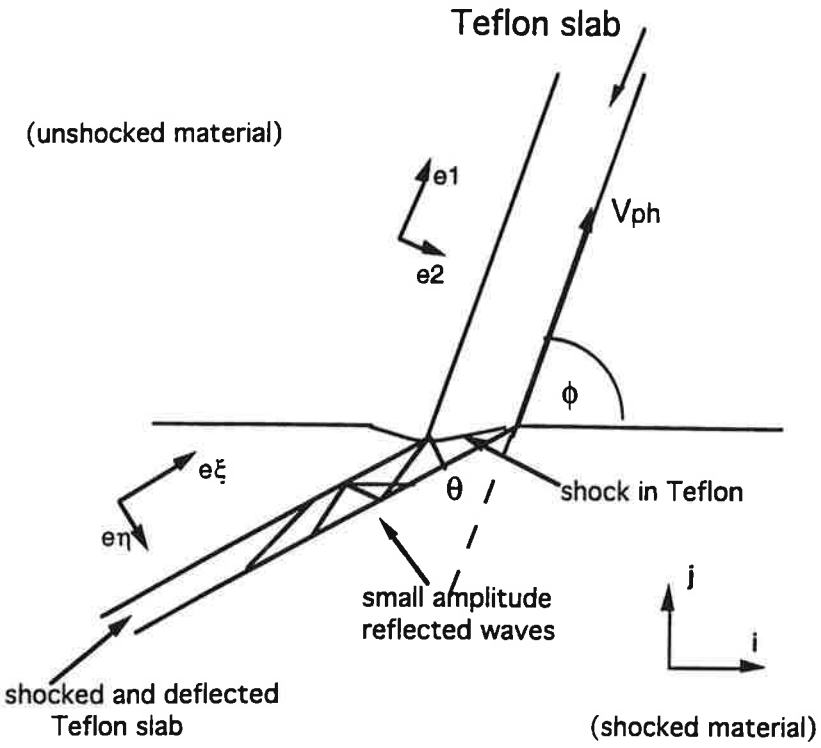

Figure 8. An expanded view of the oblique gauge/shock interaction. The small amplitude reflected waves are neglected in this analysis. The case of supersonic flow as seen by an observer traveling at V_{ph} is considered.